524 KSME International Journal, Vol. 13, No. 7, pp. 524~535, 1999

# Impact Damage and Hygrothermal Effects on Fatigue Bending Strength of Orthotropy Composite Laminates

**Kwang-Hee Im*, Kim Sun-Kyu** and In-Young Yang*****

*(Received June 1, 1998)*

This paper focuses on fracture mechanisms experimentally based on the scanning acoustic microscope (SAM) when subjected to impact damages, i. e., foreign object damages (FOD), and also on the influence of impact damages and hygrothermals on residual fatigue bending strength of CFRP laminates. Composite laminates used in the experiments are CF/Epoxy orthotropy laminated plates, $[0_4/90_4]_S$. A steel ball launched by an air gun impacts on CFRP laminates to generate impact damages. Bending fatigue tests are periodically interrupted for a nondestructive evaluation (NDE) measurement of the progressive damages to build the fracture mechanism based on impact damages, and three-point fatigue bending tests are carried out to investigate the influence of hygrothermals on the effect of the residual bending fatigue strength of CFRP laminates.

**Key Words:** Hygrothermals, Moisture Absorbtion Content, Foreign Object Damages (FOD), Impact Damages, Carbon-Fiber Reinforced Plastics (CFRP), Impact Energy, Residual Fatigue Bending Strength

## 1. Introduction

Currently the importance of carbon-fiber reinforced plastics (CFRP) in both space and civil aircraft, which require superior stiffness and strength, has been generally recognized, and CFRPs are widely used due to the ultimate light weight compared to conventional metallic materials (Lubin, 1982).

Unfortunately, CFRP laminates are brittle for dynamic loadings, particularly impact loading (Tanaka and Kurokawa, 1989), which can significantly detiorate their properties, and therefore the impact problems of composites are becoming important. A dropped wrench, bird strike (Ma et al., 1991) or runway debris can generate local delaminated areas of foreign object damage (FOD) (Takeda, 1985, and ASTM, 1973) by an impact. It is frequently difficult to detect damage with areas naked eyes. Though this damage may seem Innocuous in the stacking plates, it can result in premature catastrophic failure due to the decreasing strength caused by impact loading. Also the deformation of the CFRP composite laminates is also possible with change of temperature and absorption of moisture (Tsai, 1980) due to susceptibility to hygrothermals, especially on the matrix material. Hygrothermals can result in deformation in composite laminates, for example, interface properties which indicate the static and fatigue bending strength of the CFRP laminates (Challenger, 1986).

Recently fatigue tests are widely performed using FRP laminates and notched laminates in the case of FRP members subjected to cycle loadings. Rotem (Rotem et al., 1990), Bakis (Bakis et al., 1985) and Smith (Smith and Grove, 1987 and Im et al., 1996) have studied only the decreasing relationships of fatigue strength using composites

* Factory Automation Research Center for Parts of Vehicles Chosun University 375 Seonam-dong, Dong-gu Kwangju 501-759, Korea
** Department of Automobile Engineering Iksan National College, Iksan Chollabukdo 570-110, Korea
*** School of Mechanical Engineering and Factory Automation Research Center for Parts of Vehides, Chosun University 375 Seonam-dong, Dong-gu Kwangju 501-759, Korea

under cycle loadings. And in the case of composite laminate subjected to hygrothermals, the decrease of residual strength has been studied (Sirkis, Chang and Smith, 1994 and Yang et al., 1994).

In the study after a steel ball is impacted on the CFRP laminates, the static and fatigue bending strength are estimated, and the failure mechanisms are confirmed on the basis of damage developments, which are observed by SAM. The influence of moisture content on the fatigue bending strength is investigated with the composite laminates under hygrothermals.

This paper also attempts to evaluate the residual fatigue bending strength of laminates through a three-point bending fatigue test, to investigate moisture absorption characteristics on the fatigue bending strength under hygrothermals and to confirm failure mechanisms based on damage development.

## 2. Moisture-Absorbtion Theory

Thermal conduction equation of unidirectional fiber-reinforcement composite materials is as follows (Stephen and Hahn, 1980)

$$q^T = -D^T T \tag{1}$$

where $q^T$ is the heat efflux, $D^T$ is the thermal conduction and $T$ is the temperature gradient.

Consider an infinitesimal element dz, the governing equation for T can be obtained from the energy as shown in Fig. 1.

$$q_z^T - (q_z^T + \frac{\partial q_z^T}{\partial z} dz) = \rho C \frac{\partial T}{\partial t} dz \tag{2}$$

where $q_z^T$ is the heat efflux, $\rho$ is the density and C is the specific heat.

Substitution of Eq. (1) into Eq. (2) leads to;

$$\frac{\partial}{\partial z}(D_z^T \frac{\partial T}{\partial z}) = \rho C \frac{\partial T}{\partial t} \tag{3}$$

where $D_z^T$ and $\rho C$ are constant. Eq. (3) can be reduced to

$$\frac{D_z^T}{\rho C} \partial^2 \frac{T}{\partial z^2} = \frac{\partial T}{\partial t} \tag{4}$$

If the moisture diffusion is applied to the infinite-flat plate on assumption that the moisture diffusion is through the thickness to Eq. (4), Fick's equation becomes as follows (Ishai and Arnon, 1978)

$$D_z \frac{\partial^2}{\partial z^2} M = \frac{\partial M}{\partial t} \tag{5}$$

where M is the moisture concentration, $D_z$ is the moisture diffusion coefficient to z-direction and t is the time.

Boundary conditions of Eq. (5) are as follows;

$$M = M_0 \ at \ t \leq 0 \text{ and } 0 < z < h$$
$$M = M_\infty \ at \ t > 0 \text{ an } z = 0, \ z = h \tag{6}$$

where h is the thickness of laminates and z is the thickness direction of laminates as shown in Fig. 1.

The solution to Eqs. (5) and (6) is given as follows

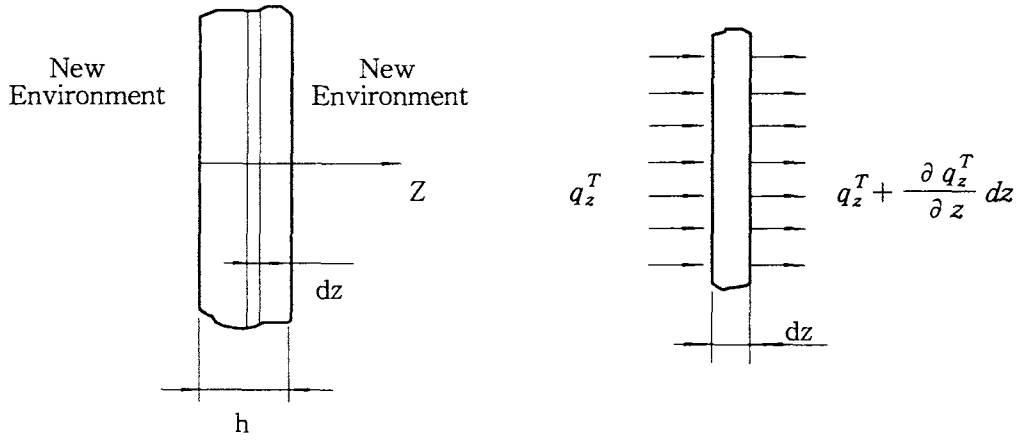


**Fig. 1** A thin laminate subjected to the environmental change.

$$\frac{M-M_0}{M_\infty-M_0}=1-\frac{4}{\pi}\sum_{j=0}^{\infty}\left\{\frac{1}{2j+1}\sin\frac{(2j+1)\pi z}{h}\exp\left[-\frac{\pi^2 Dt}{h^2}(2j+1)^2\right]\right\} \quad (7)$$

Integration of Eq. (5) with respeat to the thickness of laminates results in moisture content G of laminates as follows

$$G=\int_0^h M(z,\ t)\,dz \quad (8)$$

The moisture content G can be obtained from Eqs. (5), (6) and (8).

$$G=\frac{M-M_0}{M_\infty-M_0}=1-\exp\left[-7.3\left(D_z\frac{t}{h^2}\right)^{0.75}\right] \quad (9)$$

Also, the moisture-absorbed rate of laminates is as follows (Whitney et al., 1984)

$$M=\frac{W_m-W_d}{W_d}\times 100 \quad (10)$$

where $M$ is the moisture absorbtion rate (%), $W_d$ is the laminate weight before absorption (g) and $W_m$ is the laminate weight after absorption (g).

The laminates are weighed to determine the moisture content which is the total mass of the absorbed moisture divided by the dry weight of the laminates. The moisture content is in fact the same as the average specific moisture concentration $\bar{M}$ defined by

$$\bar{M}=\frac{1}{h}\int_0^h M\ dz \quad (11)$$

Substituting Eq. (7) into Eq. (11) and noting that

$$\bar{M}=M_0 \text{ for } t=0$$
$$\bar{M}=M_\infty \text{ for } t=\infty \quad (12)$$

We obtain from Eqs. (7) and (11).

$$\frac{\bar{M}-M_0}{M_\infty-M_0}=1-\frac{8}{\pi^2}\sum_{j=0}^{\infty}\left\{\frac{1}{(2j+1)^2}\exp\left[-\frac{\pi^2 Dt}{h^2}(2j+1)^2\right]\right\} \quad (13)$$

For sufficiently large t Eq. (13) can be approximated by the first term in the series.

$$\frac{\bar{M}-M_0}{M_\infty-M_0}=1-\frac{8}{\pi^2}\exp\left(-\pi^2\frac{Dt}{h^2}\right) \quad (14)$$

On the other hand, for short times an approximation can be obtained as follows

$$\frac{\bar{M}-M_0}{M_\infty-M_0}=4\left(\frac{Dt}{\pi h^2}\right)^{\frac{1}{2}} \quad (15)$$

Also, we can determine the moisture diffusion coefficient D from Eq. (15) as

$$D=\frac{\pi}{16}\left(\frac{\bar{M}_2-\bar{M}_1}{M_\infty-M_0}\right)^2\left(\frac{h}{\sqrt{t_2}-\sqrt{t_1}}\right)^2 \quad (16)$$

where $h$ is the thickness of laminates (mm).

## 3. Experimental Method

### 3.1 Specimen configuration

The laminates of specimens are manufactured from one-directional prepreg sheets of T300-3000 carbon fibers, #2500 EPOXY resin (CF/Epoxy) in Japan Toray P3051-15, cured to the manufacturer's specification. Its lay-up, stacked with 16 plies is $[0_4/90_4]_S$. Test specimens are prepared with dimensions 40mm×180mm×2.5mm (width×length×thickness). Prepreg sheets are composed with about 37% resin and 63% fiber contents.

The fiber direction of specimen surface is manufactured to correspond to a direction of 0°; thus, the fiber direction is the same as the length direction. By regulating the width of unimpacted specimens larger than that of specimens generated by an impact load, it is possible that none of the results of experimentation are influenced by the edge effects. By properly manipulating the hardening temperature point with the use of a heater at the vacuum bag of autoclave, the CFRP laminates can be cured.

### 3.2 Impact experimentation

The test fixture consisted of two steel plates (10 mm in thickness) and two rubber plates (10mm in thickness), which are cut with a circular hole (150mm diameter) at the center of plates, and the specimen is mounted in the space between the rubber plates with the steel plates on each side. A steel ball 5mm in diameter (0.5g) was impacted on the specimen by using compressed air as shown in Fig. 2.

The velocity of the steel ball is measured just

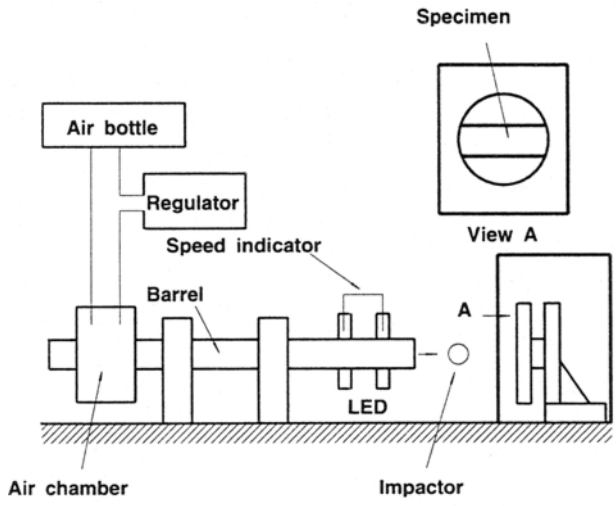


**Fig. 2** Schematic of experimental setup.

before impact by measuring the time taken for it to pass two fine laser beams located a known distance (10mm) apart. The impact velocity is obtained by varying air pressures on a compressor. The impact energy is about 1.71J (with a velocity of 82.64m/s). The impact energy (J) shows the kinetic energy of the impactor prior to impact.

### 3.3 Damage detection techniques

After impact, the delamination of specimen interfaces is assessed using an ultrasonic microscope (Olympus UH100 with the range of 30MHz). Fatigue three-point bending tests are periodically stopped for the impact-induced progressive damage from the fixture and the test is performed again. After labeling each interface A and B from the impact point as shown in Fig. 9, interface A on the impacted side is observed in the case of specimen and interface B on the opposite impacted side is observed.

The measurement methods for the delamination area are as follows; each interface is classified according to colors and the distributed range of each color is measured using the ultrasonic microscope. The ultrasonics of frequency such as a high -frequency voltage is sent to the piezo transducers on the acoustic lens and the ultrasonics can be convergent due to the spherical section of acoustic lens. In order to magnify the medium from the lens, water greater than density of air is used as a couplant.

### 3.4 Fatigue three-point bending test

To examine residual bending fatigue strength of the specimen subjected to impact damages and to observe the damage growth in the specimens, a fatigue three-point bending test is carried out. Figure 3 shows a mounting method of specimens in impact test. Figure 4(a) shows the fixture attached to the universal testing machine (Instron 8501) for the experiments of impacted-side tension and compression, respectively. Also, static and fatigue bending tests are carried out under the hygrothermals according to moisture absorbtion contents (0%, 0.2%, 0.7%, 1.5%). Fig. 5 shows the schematic of the three-point bending fatigue test under water. Distilled water at a temperature of 55℃ ($\rho > 50k\Omega \cdot m$, specfic resistance) is used to accelerate the moisture absorbtion rate and the moisture absorbtion content was measured at regular intervals up to the time moisture reaches a saturated level. Before the moisture test, the prepared specimens are stored in the vacuum oven (Model 5831, 30 inHg, Napco) at an atmospheric temperature of 80℃ for 24 hours to remove the internal moisture of the laminates, and the specimens are cooled down with the silica gel desiccator[Dewimile, 1980]. The moisture absorbtion contents are accurately measured for every tests

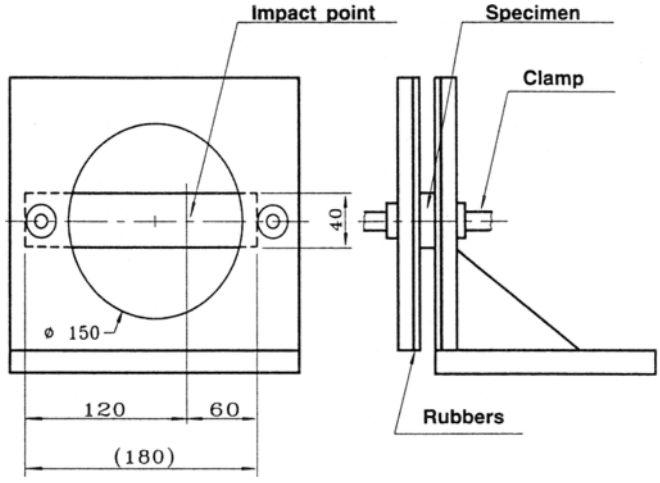


**Fig. 3** Supporting method of specimens.

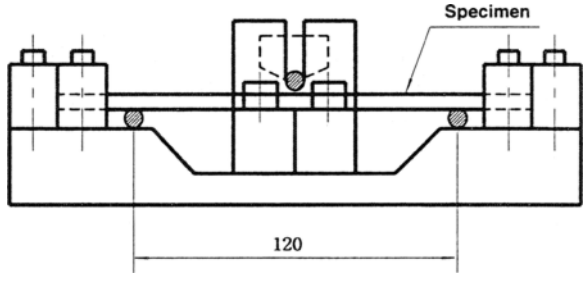


(a) Bending fixture

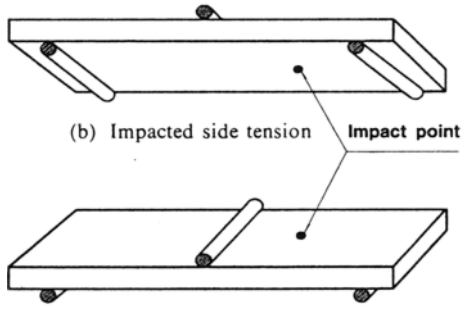


(c) Impacted side compression

**Fig. 4** Specimen supporting fixture for three-point bending test.

using the electronic scale (max. measuring range, 1/100,000g). When taking moisture weight, the moisture absorbtion content is plotted by percentage (1/100), %. The fatigue three-point bending tests are performed when the moisture absorbtion contents of specimens are 0%, 0.2%, 0.7%, 1.5%.

The fatigue test conditions are as follows : loading form is sine wave, loading ratio is 0.1 and frequency is 1.5 Hz. In the fatigue bending test, the maximum loading and bending stresses are measured when the specimen is fractured during the fatigue test.

The fracture bending stresses are measured on the assumption that the specimen are homogeneous isotropic materials (Malvern et al., 1989) because the stresses of CFRP laminates are linearly proportional to strain up to the point of rupture. The effects of dimension error can be

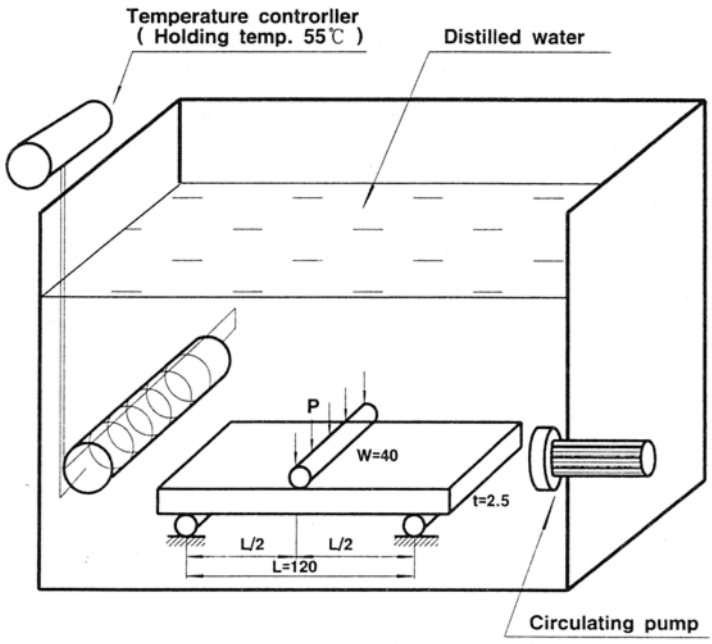


**Fig. 5** Test arrangement of three-point bending fatigue test under water.

eliminated by using a true measurement (i. e., at a width and thickness of a specimen).

The fracture bending stress equation is

$$\sigma=\frac{(PL/4)(d/2)}{I}=\frac{3PL}{2bd^2}$$

$$I=\frac{bd^3}{12} \tag{17}$$

where $\sigma$ is the bending stress (Pa), **P** is the maximum loading at fracture (N), **L** is the length of span (m), **b** is the width of specimen (m), **d** is the thickness of specimen (m), and **I** is the moment of inertia ($m^4$).

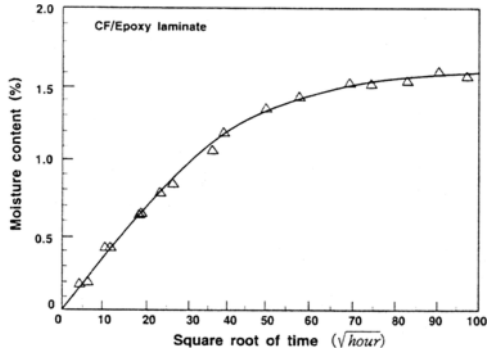


**Fig. 6** Moisture content as a function of time under hygrothermals.

## 4. Results and Discussion

### 4.1 Moisture absorption behavior under hygrothermals

To investigate the influence of moisture content on the fatigue bending strength when the composite laminates are subjected to hygrothermals, the static and fatigue bending strengths of laminates are estimated according to the moisture content under the distilled water of temperature 55℃.

Figure 6 shows the moisture content with the variation of time and the curve is plotted with using a method of least squares. Rapid moisture content diffusion appears at the initial time, but with time the moisture-content diffusion becomes slow. The moisture content diffusion attains at the moisture saturation levels. To formulate the moisture absorbtion content rate of the composite laminates with time, the equation $M(\%)=\alpha+\beta \mathrm{Ln}\sqrt{hr}$. is the most useful in all equations as a method of least squares, where $\alpha$ is $-0.64$ and $\beta$ is 0.47. Eq. (7) is shown graphically in Fig. 7 where the nondimensional time $Dt/h^2$ is used. Note that M eventually reaches $M_\infty$ throughout

the experimental data in Fig. 8. It is thought that ananlytical solutions agree well with experiments for the moisture content. Therefore Eq. (16) is applicable when obtaining the moisture diffusion coefficient, which indicates the moisture development conditions. By using the moisture data for the composite laminates we have obtained the moisture diffusion coefficient in Table 1. When solving the moisture diffusion coefficient the linear region was chosen and the coefficient was obtained between two moisture contents $M_1$ and $M_2$ corresponding to $t_1$ and $t_2$, respectively, where $t_1$ is 180 hours and $t_2$ is 70 hours in this experiment.

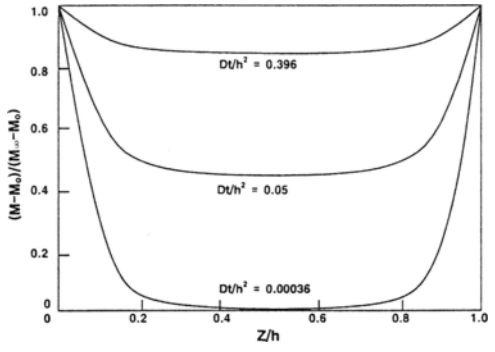


**Fig. 7** Moisture profile as a function of time with variations of nondimensional time.

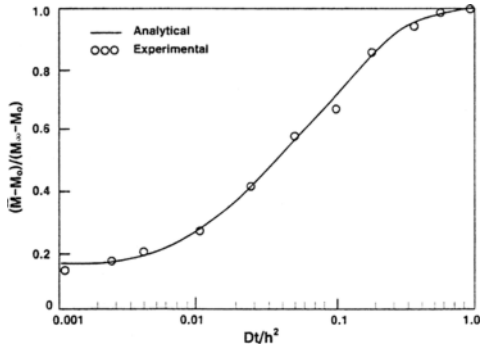


**Fig. 8** Experimental correlation with variations of nondimensional time.

### 4.2 Observation of progressive damage from impact

In the case of impact-induced CFRP laminates subjected to cyclic loadings, initial impact damage in the interfaces is observed by using SAM to build up the failure mechanisms and impact -damaged growth is observed in every specified cycle until fractured.

Figure 9 shows the typical delamination shape of the specimen, and A and B indicate interfaces A and B respectively. Figure 10 shows the progressive damage direction in the case of impact -side tension when carrying out the three-point fatigue bending test, and Fig. 10 (a), (b) and (c) indicate the delamination shapes after 0, 10,000 and 20,000 cycles, respectively. Figure 11 shows the damage growth direction in the case of impact-side compression, and Fig. 11(a) and (b) indicate the delamination shapes after 0 and 20, 000 cycles, respectively. From the Fig. 10 (b) and (c), fracture developes toward the impact point from the edge of interface B delamination after 10, 000 cycles, the damaged-growth width increases from the edge after 20,000 cycles and finally the specimen is fractured after 21,000 cycles. On the other hand, Fig. 11 shows that fracture propagat-

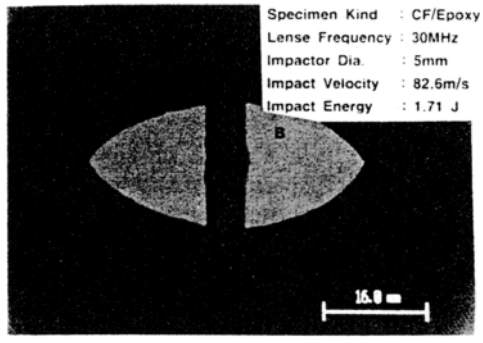


A : The 1st interface from the impact point
B : The 2nd interface from the impact point

**Fig. 9** Typically delamination shape from impact-induced damages.

**Table 1** Diffusion coefficient (D).

| Symbols / Types | Moisture time (t) | | Moisture rate (M) | | $M_\infty$ (%) | Thickness (h) | D ($mm^2$/sec) |
|---|---|---|---|---|---|---|---|
| | $t_2$ | $t_1$ | $M_2$ | $M_1$ | | | |
| CF/Epoxy | 180 | 70 | 0.501 | 0.304 | 1.501 | 2.610 | $16.6 \times 10^{-8}$ |

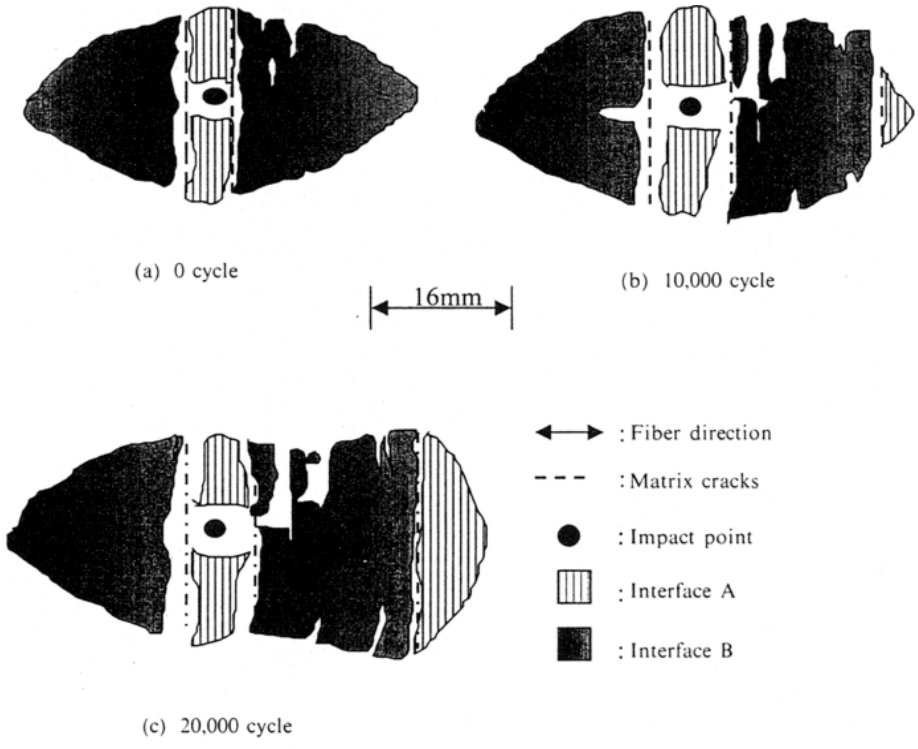


**Fig. 10** Progressive damage during fatigue bending test when the impacted side is tensioned.

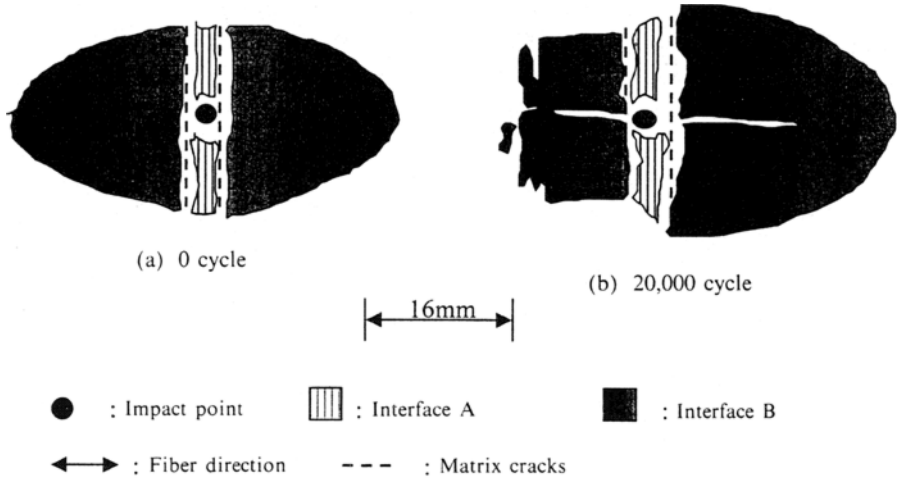


**Fig. 11** Progressive growth during fatigue bending test when the impacted side is compressed.

ed from the transverse crack near the impact point in the case of impact-side compression and eventually fracture is generated along the transverse crack after 20,600 cycles.

### 4.3 Relationslip between residual fatigue bending strength and impact damages for moisture content

After observing the interface damage range of

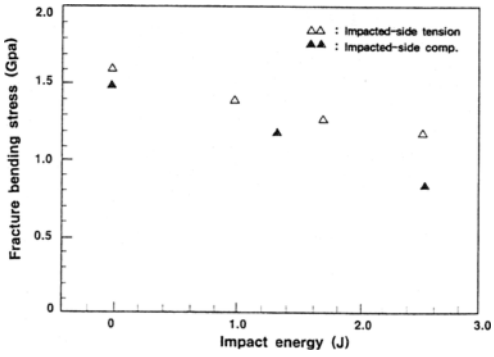


**Fig. 12** Relation between impact energy and fracture bending stress.

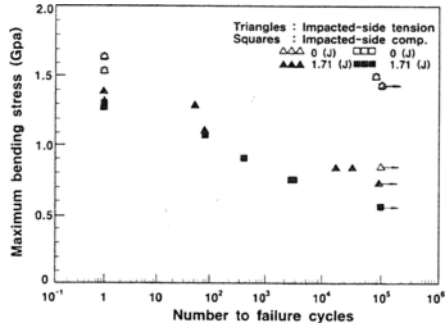


**Fig. 13** Residual fatigue bending strength of damaged specimens.

the specimens with impact damage by SAM, the static three-point bending test is performed to consider the decreasing relation of residual bending strength.

Figure 12 shows the relation between impact energy and fracture bending stress of specimens for each case of impact-side tension and compression. Using a true measurement and loading at the breaking point of the specimen, residual bending strength is solved by Eq. (17). The strength in the case of impact-side compression decreases much more than that in the case of impact-side tension if the case of impact-side tension is compared with that of impact-side compression. Figure 13 shows the fatigue test results of specimens for each case of impact-side tension and compression. The Y-axis indicates the maximum bending stress, the X-axis indicates the number of cycles to failure and an arrow (→) indicates runway. From the results of the fatigue tests, the fatigue strength in impact-side compression decreased more than

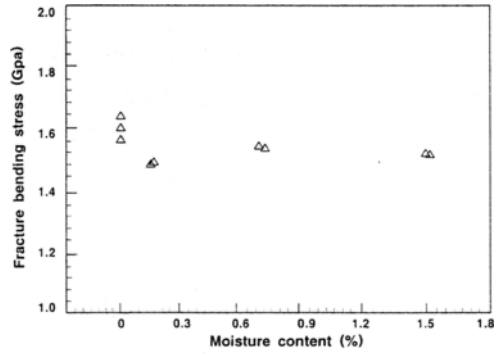


**Fig. 14** Relation between fracture bending stress and moisture content.

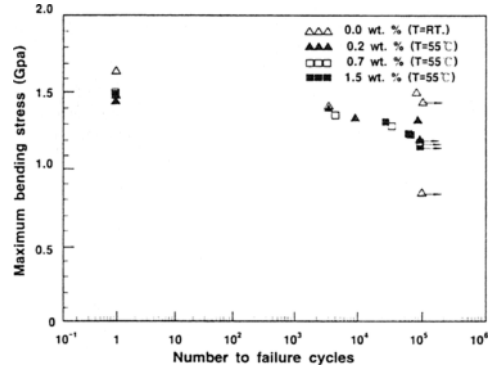


**Fig. 15** Residual fatigue bending strength variations according to moisture absorbtion contents.

that in impact-side tension as in the results of the static bending test shown in Fig. 12 because the matrix cracks generated at an impact point affect the fatigue bending strength.

The fracture bending stress and residual fatigue bending strengths are estimated according to moisture conditions of the laminates. From Fig. 14, the rapid strength decreasing phenomena appear at approximately 0.2% if compared with those of no-moisture conditions. Even through the moisture rate increases over 0.2%, decreasing phenomena of bending strength do not appear to time the moisture contents become to be 0% and 1.5%.

Figure 15 shows the residual fatigue bending strength when the composite laminates are subjected to the hygrothermals (0%, 0.2%, 0.7%, and 1.5% moisture content). At the no-moisture

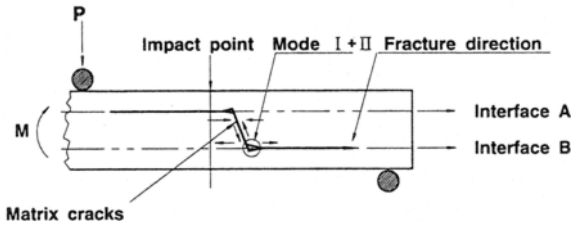


(a) Progressive damage mode

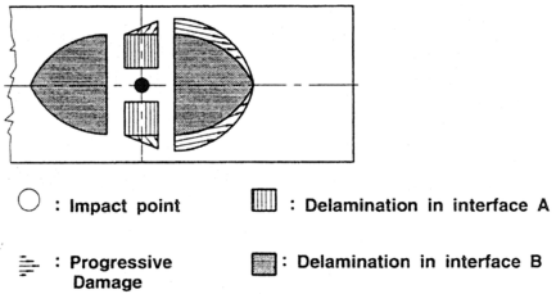


(b) Progressive damage direction

**Fig. 16** Mechanism of pregrossive damage during fatigue bending test when the impacted side is compressed.

condition, approximately 11% of fatigue bending strength decreases. Bending strength decreased approximately 10% for specimen at about 0.2% moisture absorbtion compared with that of no -moisture conditions. Also, bending strength decreased approximately 3.8% and 5.73% at moisture contents of about 0.7% and 1.5%, respectively, compared with that of no-moisture conditions. Especially, at a moisture rate of approximately 0.2%, fatigue bending strength decreases greatly about 10% compared with the static bending strength because the moisture affects the matrix along the fibers. It is therefore thought that moisture diffusion greatly effects the residual fatigue bending strength more than the static bending strength when subjected to the hygrothermals.

### 4.4 Failure mechanism from impact-induced damages

As described in Sec. 4 · 1, damage growth is observed by SAM to study the decreasing relation of residual fatigue bending strength of specimen for each case of impact-side tension and compression. Especially in the case of specimens where the residual fatigue bending strength is radically decreased, it is clear that the fractures grew at the transverse cracks, which occurred at an impact point by total delamination of the interface B (90°/ 0°) under tension as shown in Fig. 16 for impact-side compression. Also, it is found that the delamination width of the interface B increased during damage growth.

In the case of impact-side tension as shown in Fig. 10, the transverse cracks are generated at the delamination edge of the interface B. Contrary to impact-side compression, it is shown that the specimen fractures grew from the transverse cracks to the impact point as the cyclic loadings repeated. In case of impact-side compression only where radically decreasing bending strength occurs, Fig. 16 shows the fracture modes by conducting the fatigue bending test from the damaged-growth shapes of Fig. 11, using the specimens subjected to impact damages and also shows the delamination growth direction.

Figure 16 shows the failure mechanism during fatigue bending test when the impacted side is under the compression. Here, Fig. 16(a) exhibits a progressive damage direction and Fig. 16(b) exhibits a progressive damage mode based on the delamination and fracture surface growth of an

ultrasonic microscope in fatigue tests. In the case of impacted-side compression, shown in Fig. 16, the delaminations of interfaces A and B grew along the transverse cracks generated below the impact point, and the delamination possessing the greatest growth width is the delamination for the interface B on the tension side. To explain the phenomenon, Fig. 16(a) shows in details the fracture growth modes in consideration of shear stresses, tension and compression in the plane. When the transverse cracks extend in the tension direction in these modes, opening displacement becomes greater, and when the cracks extend in the compression direction, closing phenomena occur. Thus, because the opening displacements on the tension side (modes Ⅰ + Ⅱ) are higher than those on the compresion side, delamination on the tension side can easily extend. Therefore, when the delamination develops in each ply, the interface modes can be assumed as shown in Fig. 16(a). The cause of transverse cracks occurring from impact loading reveals that the delaminations grew from the shearing strain generated during the three-point bending test. Figure 16(b) shows the delamination, and fracture surface growth direction.

Therefore, the delamination and the growth direction can be assumed as shown in Fig. 16 (a), and delamination growth by shear strain causes each interface to fail. Figure 16(b) shows the delamination and the growth direction. Also, in the case of impact-side tension shown in Fig. 10, matrix cracks occur at the delamination edge of the interface B on the compression side and it is known that the delamination of the interface B grew toward the impact point. Thus, as shown in Fig. 16, the moment becomes greater because the curvature at the fracture starting point is smaller in the case of impact-side tension than in the case of impact-side compression from the impact point. Therefore, it is known that more fractures develop immediately under impact-side compression than under impact-side tension. Also, shock resistance of impact-side tension is greater than that of impact-side compression when CFRP laminates are subjected to impact damages

## 5. Conclusion

After impact test of the CFRP laminates, impact-induced progressive damage is observed and the residual strength of the static and fatigue three-point bending test was evaluated. The phenomena of decreasing residual strength and the failure mechanisms were analyzed. Also, the moisture absorbtion characteristics and influence of moisture content were investigated when the composite laminates were subjected to hygrothermals. The conclusions are as follows:

(1) It has been found that the phenomenon decreasing of residual fatigue bending strength in the case of impact-side compression appears greater than the case of impact-side tension for the orthotropic composite laminates.

(2) In the case of impacted-side compression, fracture is propagated from the transverse crack generated near the impact point. On the other hand, fracture develops toward the impact point from the edge of the interface B delamination in the case of impact-side tension.

(3) At approximately 0.2% of moisture content, the phenomena of rapid strength decrease appear and the strength variations do not occur at a moisture content of over 0.2%. Also, the diffusion coefficient D can sucessfully be obtained.

(4) It is known that impact-induced damages and hygrothermals have an affect on the decreasing phenomena of residual fatigue strength to some degree. Approximately 20% in the decreasing phenomena of residual fatigue strength appears in the case of impact-side compression and about 10% of residual fatigue strength decrease occurs due to the hygrothermals.

## References

ASTM, 1973, Foreign Object Impact Damage to Composites, *STP568*. pp. 2160~2190.

Bakis C. E. and Stinchcomb W. W. (Hahn H. H), 1989, "Response of Thick, Notched Laminates Subjected to Tension-Compression Cycle Loads," *Composite Materials : Fatigue and Fracture*, ASTM STP, 907, pp. 314~438.

Challenger K. D., 1986, "The Damage Tolerance of Carbon Fiber Reinforced Composites," A Workshop Summary, *Composite Struct.*, pp. 295~318.

Dewimille B., Tjoris J., Mailfert R. and Bunsell A. R., 1980, "Hygrothermal Aging of an Unidirectional Epoxy Composites During Water Immersion," *Advances in Composite Materials*, Vol. 1, pp. 597~612.

Im K. H., Sim J. K. and Yang I. Y., 1996, "Impact Damages and Residual Bending Strength of CFRP Composite Laminates Subjected to Impact Loading," *KSME International Journal*, Vol. 10, No. 4, pp. 423~434.

Ishai O. and Arnon V., 1978, "Instantaneous Effects of Internal Moisture Conditions on Strength of Glass-Fiber-Reinforced Plastics," *ASTM*, pp. 267~276.

Lubin G., 1982, "Handbook of Composites, Van Nostrand Reinhold," p. 147.

Ma C. C. M., Huang Y. H., and Chang M. J., 1991, "Hygrothermal Effect on the PEEK/C. F. and PPS/C. F. under Impact Loading( Ⅰ )," *ANTEC*, pp. 2029~2096.

Malvern L. E., Sun C. T. and Liu D., 1989, "Delamination Damage in Central Impacts at Subperformation Speeds on Laminated Kevlar/Epoxy Plates," *ASTM. STP.* 1012, pp. 387~405.

Rotem A. and Nelson H. G., 1990, "Residual Strength of Composite Laminate Subjected to Tensile-Compressive Fatigue Loading," *Journal of Composites Technology & Research*, Vol. 12, No. 2, pp. 76~84.

Smith B. W. and Grove R. A., 1987, "Determination of Crack Propagation Directions in Graphite/Epoxy Structures," *Composites and Metals*, ASTM. STP. 948, pp. 154~173.

Sirkis J. S., Chang C. C. and Smith B. T., 1994, "Low Velocity Impact of Optical Fiber Embedded Laminated Graphite/Epoxy Panels. Part Ⅰ : Macro-Scale," *Journal of Composite Materials*, Vol. 28, No. 14, pp. 1347~1371.

Stephen W. and Hahn H. T., 1980, *Introduction to Composite Materiale*, Technomic Publishing C., Inc., pp. 329~340.

Takeda T., 1985, "Impulsive Response and Fracture of Composites ( Ⅰ )," *Journal of the Japan Society for Composite Materials*, Vol. 11, No. 4, pp. 151~161.

Tanaka T., Kurokawa T., etc., 1989, "Damage and Residual Bending Strength of Graphite/Epoxy Composite Laminates Subjected to Normal Impact," *Journal of the Japan Society for Aeronautical & Space Sciences*, Vol. 37, No. 25, pp. 29~36.

Tsai S. W. and Hahn H. T., 1980, *Introduction to Composite Materials*, Technomic Publishing Co., Inc., pp. 329~376.

Whitney J. M., Daniel I. M. and Pipes R. B., 1984, *Experimental Mechanics of Fiber Reinforced Composite Materials*, Prentice-Hall, Inc., pp. 250~255.

Yang I. Y., Matsumoto H., Adachi T., 1994, "Impact Damages of CFRP Laminates Subjected to High Temperature Atmosphere," *JSME (A)*, Vol. 60, No. 571, pp. 841~845.